

# Probing dark matter annihilation in the Galaxy with antiprotons and gamma rays

Alessandro Cuoco,<sup>a</sup> Jan Heisig,<sup>a</sup> Michael Korsmeier<sup>a,b,c</sup> and Michael Krämer<sup>a</sup>

<sup>a</sup>Institute for Theoretical Particle Physics and Cosmology, RWTH Aachen University, 52056 Aachen, Germany

<sup>b</sup>Dipartimento di Fisica, Università di Torino, via P. Giuria 1, 10125 Torino, Italy

<sup>c</sup>Istituto Nazionale di Fisica Nucleare, Sezione di Torino, Via P. Giuria 1, 10125 Torino, Italy

E-mail: [cuoco@physik.rwth-aachen.de](mailto:cuoco@physik.rwth-aachen.de), [heisig@physik.rwth-aachen.de](mailto:heisig@physik.rwth-aachen.de), [korsmeier@physik.rwth-aachen.de](mailto:korsmeier@physik.rwth-aachen.de), [mkraemer@physik.rwth-aachen.de](mailto:mkraemer@physik.rwth-aachen.de)

**Abstract.** A possible hint of dark matter annihilation has been found in Cuoco, Korsmeier and Krämer (2017) from an analysis of recent cosmic-ray antiproton data from AMS-02 and taking into account cosmic-ray propagation uncertainties by fitting at the same time dark matter and propagation parameters. Here, we extend this analysis to a wider class of annihilation channels. We find consistent hints of a dark matter signal with an annihilation cross-section close to the thermal value and with masses in range between 40 and 130 GeV depending on the annihilation channel. Furthermore, we investigate in how far the possible signal is compatible with the Galactic center gamma-ray excess and recent observation of dwarf satellite galaxies by performing a joint global fit including uncertainties in the dark matter density profile. As an example, we interpret our results in the framework of the Higgs portal model.

---

## Contents

<b>1</b>	<b>Introduction</b>	<b>1</b>
<b>2</b>	<b>Cosmic-ray fits for individual dark matter annihilation channels</b>	<b>2</b>
<b>3</b>	<b>Joint fit of antiproton and gamma-ray fluxes</b>	<b>4</b>
<b>4</b>	<b>Interpretation within the singlet scalar Higgs portal model</b>	<b>7</b>
<b>5</b>	<b>Conclusion</b>	<b>11</b>

---

## 1 Introduction

Observations of cosmic-ray (CR) antiprotons are a sensitive probe of dark matter (DM) models with thermal annihilation cross sections [1–14]. In particular, with the very accurate recent measurement of the CR antiproton flux by AMS-02 [15], it is a timely moment to investigate this subject. A joint analysis of the CR fluxes of light nuclei and a potential DM contribution to the antiproton flux provides strong DM constraints [16], as well as an hint for a DM signal corresponding to a DM mass of about 80 GeV, and a thermal hadronic annihilation cross section,  $\langle\sigma v\rangle \approx 3 \times 10^{-26} \text{ cm}^3/\text{s}$ . These values have been derived in [16] in a novel analysis where CR propagation uncertainties have been marginalized away, taking into account possible degeneracies between CR uncertainties and DM. A similar result has been found in [17], but using the boron over carbon ratio, also recently measured by AMS-02 [18]. In the present work, we shall extend the DM analysis of the CR antiproton flux presented in [16] to a comprehensive set of standard model (SM) annihilation channels, including gluons, bottom quarks,  $W$ ,  $Z$  and Higgs bosons, as well as top quarks.

Similarly, an excess in gamma-ray emission toward the center of our Galaxy has been reported by several analyses [19–30]. The spectrum and spatial distribution of this Galactic center excess (GCE) is consistent with a signal expected from DM annihilation, and consistent with the excess observed in antiprotons. The second goal which we will pursue in this work is to quantify more precisely the above statement, performing joint fits of the antiproton and gamma-ray signals for various individual DM annihilation channels. In performing this comparison we will also use the most recent results of gamma-ray observations from dwarf satellite galaxies of the Milky Way, which are a known sensitive probe of DM annihilation.

Finally, while DM annihilation can be probed in a rather model-independent way by considering individual SM annihilation channels, it is interesting to also test specific models of DM. Such models typically predict CR and gamma-ray fluxes from a combination of various SM annihilation channels, and they can be confronted with direct and collider searches for DM. As an example, we shall thus consider a minimal Higgs portal DM model, which adds a real singlet scalar DM field  $S$  to the SM. We shall demonstrate that the scalar Higgs portal model can accommodate both the CR antiproton flux and the GCE, despite strong constraints from invisible Higgs decays and direct DM detection.

The paper is organized as follows. In section 2 we analyze the CR antiproton data for individual DM annihilation channels. The joint analysis of antiproton and gamma-ray fluxes, including both the GCE and dwarf galaxies, is presented in section 3. In section 4

we consider the specific case of the scalar Higgs portal model, and present a global analysis including antiproton and gamma-ray fluxes, as well as constraints from the DM relic density, invisible Higgs decays and direct DM searches. We conclude in section 5.

## 2 Cosmic-ray fits for individual dark matter annihilation channels

DM annihilation in the Galaxy results in a flux of antiprotons from the hadronization and decay of SM particles. The corresponding source term is given by

$$q_{\bar{p}}^{(\text{DM})}(\mathbf{x}, E_{\text{kin}}) = \frac{1}{2} \left( \frac{\rho(\mathbf{x})}{m_{\text{DM}}} \right)^2 \sum_f \langle \sigma v \rangle_f \frac{dN_{\bar{p}}^f}{dE_{\text{kin}}}, \quad (2.1)$$

where  $m_{\text{DM}}$  is the DM mass and  $\rho(\mathbf{x})$  the DM density distribution. The thermally averaged annihilation cross section for the SM final state  $f$ ,  $\text{DM} + \text{DM} \rightarrow f + \bar{f}$ , is denoted by  $\langle \sigma v \rangle_f$ , and  $dN_{\bar{p}}^f/dE_{\text{kin}}$  is the corresponding antiproton energy spectrum per DM annihilation. Note that the factor 1/2 corresponds to scalar or Majorana fermion DM.

We use the NFW DM density profile [31],  $\rho_{\text{NFW}}(r) = \rho_h r_h/r (1 + r/r_h)^{-2}$ , with a characteristic halo radius  $r_h = 20$  kpc, and a characteristic halo density  $\rho_h$ , normalized to a local DM density  $\rho_{\odot} = 0.43 \text{ GeV}/\text{cm}^3$  [32] at the solar position  $r_{\odot} = 8$  kpc. The choice of the DM profile has a negligible impact on our results, as demonstrated in [16].

The energy distribution and yield of antiprotons per DM annihilation,  $dN_{\bar{p}}^f/dE_{\text{kin}}$ , is determined by the DM mass and the relevant SM annihilation channel. We use the results presented in [33] for the annihilation into gluons,  $b\bar{b}$ ,  $t\bar{t}$  and  $h\bar{h}$ . (The spectra for annihilation into light quarks are very similar to those for gluons.) For  $ZZ^*$  and  $WW^*$  final states we have generated the spectra with MADGRAPH5\_AMC@NLO [34] and PYTHIA 8.215 [35], adopting the default setting and scale choice,  $Q = m_{\text{DM}}$ . We note that the choice of the PYTHIA tune may introduce uncertainties up to about 15%, while varying the shower scale in a range between  $m_{\text{DM}}/6$  and  $2m_{\text{DM}}$  can result in uncertainties of up to 30%.<sup>1</sup> This difference is induced through the strength of the final state radiation. However, we have checked that the theoretical uncertainty in the prediction of the antiproton energy spectrum from this scale variation and different PYTHIA tunes does not affect our results. For the default PYTHIA settings, annihilation spectra into (on-shell)  $WW$  and  $ZZ$  are in reasonable agreement with those of [33].

To analyze the impact of DM annihilation on the CR antiproton flux, we perform a joint analysis of the fluxes of protons, helium and antiprotons, including a potential contribution from DM annihilation, which would affect the antiproton to proton ratio. We solve the standard diffusion equation using GALPROP [36, 37], assuming a cylindrical symmetry for our Galaxy, with a radial extension of 20 kpc. In total, we analyze a parameter space with thirteen dimensions. Eleven parameters are related to the CR sources and the propagation of CRs, while for each individual SM annihilation channel, the DM component of the CR flux is specified by the DM mass and its annihilation cross section. The parameters describing the CR sources and propagation, as well as the DM contribution, are determined in a global fit of the AMS-02 proton and helium fluxes [38, 39], and the AMS-02 antiproton to proton ratio [15], complemented by proton and helium data from CREAM [40] and VOYAGER [41]. We use MULTINEST [42] to scan this parameter space and derive the corresponding profile likelihoods. For details of the propagation model and the numerical analysis we refer to [16, 43].

<sup>1</sup>Note that in MADGRAPH5\_AMC@NLO for the default setting (dynamical scale) the scale is set to  $m_{\text{DM}}/6$ .

We use as benchmark antiproton production cross section the default in GALPROP, i.e., the parameterization from [44]. In [16] we checked recent new updated models of the cross section from [45] and [46], and we found that the results of the fit are substantially unchanged. The main effect is to slightly modify the region of parameter space preferred by DM at the level of 20–30%, leaving unchanged the values of the minimal  $\chi^2$ .

Adding a DM component significantly improves the global fit of the CR antiproton data. This is due to a sharp spectral feature in the antiproton flux at a rigidity of about 20 GV. Such a feature cannot be described by the smooth spectrum of secondary antiprotons produced by the interactions of primary protons and helium nuclei on the interstellar medium. The spectrum from DM annihilation, on the other hand, exhibits such a sharp feature from the kinematic cut-off set by the DM mass. Adding a DM component thus provides a significantly better description of the antiproton data.

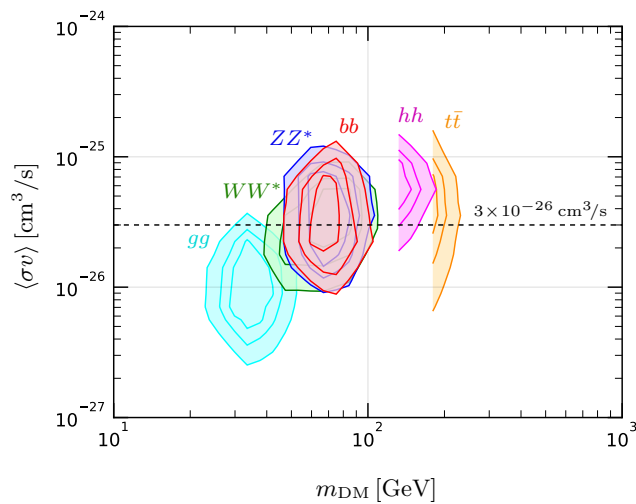


**Figure 1.** Cosmic-ray fit for the individual annihilation channels:  $gg$  (cyan),  $WW^*$  (green),  $b\bar{b}$  (red),  $ZZ^*$  (blue),  $hh$  (pink) and  $t\bar{t}$  (orange) in the  $m_{\text{DM}}-\langle\sigma v\rangle$  plane. We show the 1, 2, and 3  $\sigma$  contours. For comparison we display the thermal cross section (dashed horizontal line).

In figure 1 we present the preferred range of DM masses and annihilation cross sections for the different SM annihilation channels. The regions are frequentist contour plots of the two-dimensional profile likelihood obtained minimizing the  $\chi^2$  with respect to the remaining eleven parameters in the fit. They, thus, include the uncertainties in the CR source spectra and CR propagation. All channels provide an improvement compared to a fit without DM: we find a  $\chi^2/(\text{number of degrees of freedom})$  of 71/165 for the fit without DM, which is reduced to 46/163 ( $b\bar{b}$ ), 48/163 ( $hh$ ), 50/163 (gluons and/or light quarks), 50/163 ( $WW^*$ ), 46/163 ( $ZZ^*$ ), and 59/163 ( $t\bar{t}$ ), respectively, when adding a corresponding DM component (see also Table 1). Formally,  $\Delta\chi^2 = 25$  for the two extra parameters introduced by the DM component with annihilation into  $b\bar{b}$  corresponds to a significance of 4.5, although such an estimate does not account for possible systematic errors.

Figure 1 also shows that different annihilation channels would imply different preferred DM masses, ranging from  $m_{\text{DM}} \approx 35$  GeV for gluons and/or light quarks to  $m_{\text{DM}}$  near the Higgs and top mass for annihilation into Higgs or top-quark pairs, respectively. For all the channels, the fit points to a thermal annihilation cross section  $\langle\sigma v\rangle \approx 3 \times 10^{-26}$  cm<sup>3</sup>/s.

It can be noted that the values of the  $\chi^2$  are typically quite low for both the fits with and

without DM. This is due to the fact that CR data error-bars are dominated by systematic errors rather than statistical errors. This is true in particular for the proton and helium data, while for the antiproton to proton ratio the two errors have comparable weight. As a consequence, the use of  $\chi^2$  statistics to describe the data is not fully correct. A proper treatment would require a deeper knowledge of the systematic uncertainties so that to include them directly at the level of the likelihood rather than in the error-bars. This information is, however, not publicly available, and this approach is not possible at the moment. It would be desirable that such a more complete information is released for future CR data publications and updates.

### 3 Joint fit of antiproton and gamma-ray fluxes

DM annihilation would also result in a flux of gamma rays, predominantly from the decay of pions produced in the fragmentation of SM particles. The gamma-ray flux per unit solid angle at a photon energy  $E_\gamma$  is

$$\frac{d\Phi}{d\Omega dE} = \frac{1}{2m_{\text{DM}}^2} \sum_f \frac{dN_\gamma^f}{dE} \frac{\langle\sigma v\rangle_f}{4\pi} \int_{\text{l.o.s.}} ds \rho^2(r(s, \theta)) , \quad (3.1)$$

where  $dN_\gamma^f/dE$  is the photon spectrum per annihilation for a given final state  $f$ , and  $\langle\sigma v\rangle_f$  is the corresponding annihilation cross section. The integral has to be evaluated along the line-of-sight (l.o.s.) at an observational angle  $\theta$  towards the Galactic center. The l.o.s. integral of the DM density-squared,  $\rho^2$ , over the solid angle  $d\Omega$  is called the  $J$ -factor. We adopt a generalized NFW profile [28] with an inner slope  $\gamma \simeq 1.2$  for the DM density  $\rho$ . This is in contrast to the standard NFW profile applied in section 2. However, CRs and gamma-rays probe very different parts of the profiles. The l.o.s. integral in Eq. (3.1) is very sensitive to the profile behavior close to the Galactic center, while CRs mostly probe the local DM distribution. Indeed, in the latter case we verified that even changing to the cored Burkert profile [47] does not affect the results of the CR fit [16]. From this point of view it is legitimate to use an NFW profile for CRs while adopting the generalized NFW profile for gamma-rays.

An excess in the flux of gamma rays from the Galactic center has been reported by several groups [19–30] (but see also [48]). The GCE is peaked at photon energies of a few GeV, and consistent with a spherical morphology, extending up to at least  $10^\circ$  away from the Galactic center, and a steep radial profile [27, 28]. Various astrophysical processes have been proposed to explain the excess [49–51]. Also, studies based on photon-count statistic suggest that the excess is more compatible with a population of unresolved point sources rather than with a pure diffuse emission [52–54]. Nonetheless, a DM interpretation is still viable. In particular, the excess is compatible with the signal expected from the annihilation of DM, with a cross section close to the thermal value and with a DM mass around 50 GeV. In our analysis of the GCE we will use the gamma-ray energy spectrum and error covariance matrix obtained in [28].

DM annihilation in gamma rays can also be sensitively tested by observations of dwarf satellite galaxies of the Milky Way [55–58]. Here, we use the likelihood as a function of the flux for each dwarf provided by Fermi-LAT [58], and the gamma-ray spectra for the individual annihilation channels obtained in [59]. We consider a total of eleven dwarfs: the seven brightest confirmed dwarfs analyzed in [58] (Coma Berenices, Draco, Sculptor, Segue 1, Ursa Major II, Ursa Minor, Reticulum II) as well as Willman 1, Tucana III, Tucana IV

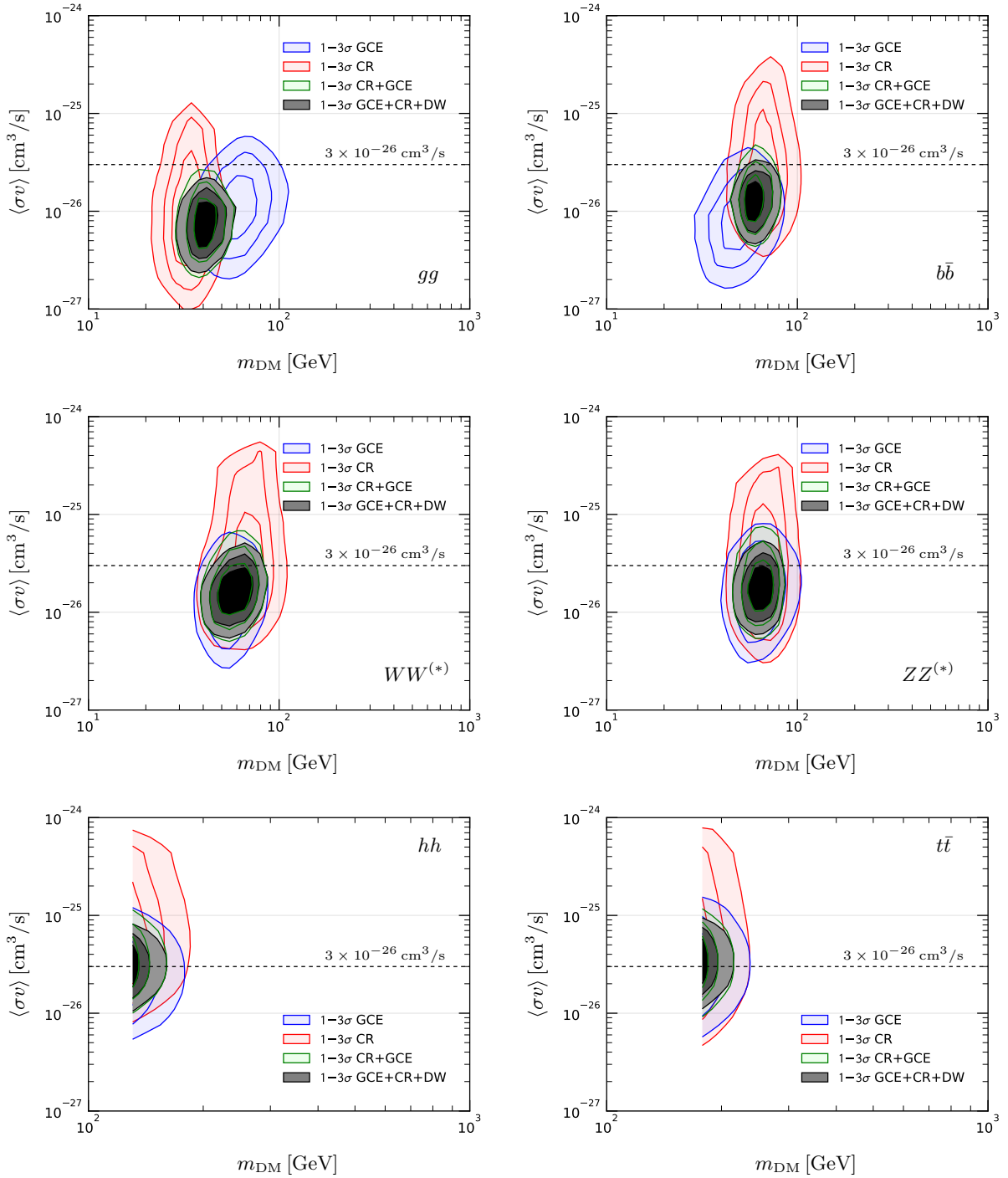


**Figure 2.** Joint fit to CR fluxes, the GCE and dwarf galaxies for the individual SM annihilation channels in the  $m_{\text{DM}}-\langle\sigma v\rangle$  plane. We show the 1, 2, and 3  $\sigma$  contours. For comparison we display the thermal cross section (dashed horizontal line).

and Indus II. Four of these dwarfs (Reticulum II, Tucana III, Tucana IV, Indus II) exhibit small excesses at the level of  $\sim 2\sigma$  (local) each, which are compatible with a signal from DM annihilation with a thermal cross section [58, 60, 61]. The total likelihood is obtained as a product of likelihoods over each single dwarf as described in [57, 62]. The likelihood of each dwarf contains a factor from the flux likelihood, and a log-normal factor from a deviation of the  $J$ -factor from its nominal value. For the seven brightest confirmed dwarfs we use the  $J$ -factors and corresponding uncertainties provided in [58] (which, in turn, draws from [63], except for Reticulum II, whose  $J$ -factor is taken from [64]), while for Willman we use the  $J$ -factor from [57]. For Tucana III, Tucana IV and Indus II we use the distance-based predictions provided in [58] with a medium estimated error of 0.6 dex. We marginalize over the  $J$ -factors of the individual dwarf galaxies in the fit. It should be noted that estimates of the  $J$ -factors present some differences depending on the analysis (compare for example [63, 65]), with some analysis [66] finding somewhat lower values than the others. This, however, has only a minor impact on our results, since, as we show below, the results of the fits are dominated by the GCE and CR signals.

On the basis of the likelihoods obtained in the CR fit described in section 2 we now perform a joint fit of CR antiprotons and of gamma-rays from the Galactic center and from dwarf galaxies. The gamma-ray fit follows the methodology described in [59]. The fit contains four input parameters, the model parameters,  $\langle\sigma v\rangle$  and  $m_{\text{DM}}$ , as well as the  $J$ -factor for the Galactic center,  $\log J$ , and the local DM density  $\rho_{\odot}$ . The latter two parameters are, in principle, not independent. However, as already mentioned above, CRs and gamma-rays probes different parts of the DM distribution in the Galaxy and it is thus reasonable to explore the uncertainties in these two parameters as independent. For  $\log J$  we use a gaussian distribution (log-normal in  $J$ ) with mean 53.54 and error 0.43, i.e.,  $\log(J/\text{GeV}^2\text{cm}^{-5}) = 53.54 \pm 0.43$ . This GC  $J$ -factor refers to an integration region of  $40^\circ \times 40^\circ$  around the GC and with a stripe of  $\pm 2^\circ$  masked along the Galactic plane, in order to be compatible with the GCE data from Ref. [28] that we use. The details of the derivation of the distribution in  $\log J$  and the error are described in [59]. For the local DM density we also use Gaussian errors  $\rho_{\odot} = 0.43 \pm 0.15 \text{ GeV}/\text{cm}^3$  [32]. We use the result of Ref. [32] in order to be conservative since  $\rho_{\odot}$  has a relatively large error. A recent review on the status of the determination of  $\rho_{\odot}$  is given in [67].

Figure 2 shows the preferred range of DM masses and annihilation cross sections, where we have marginalized over  $\log J$  and  $\rho_{\odot}$ . We present 1, 2, and 3  $\sigma$  contours for a fit to the GCE (blue), CR (red), CR+GCE (green) and CR+GCE+dwarfs (black) for the six annihilation channels  $gg$ ,  $b\bar{b}$ ,  $WW^{(*)}$ ,  $ZZ^{(*)}$ ,  $hh$  and  $t\bar{t}$ . Note that the fits to the CR fluxes in figure 2 show a wider spread in  $\langle\sigma v\rangle$  than those displayed in figure 1, because in figure 2 we marginalize over the local DM density,  $\rho_{\odot} = 0.43 \pm 0.15 \text{ GeV}/\text{cm}^3$ , while in figure 1 a fixed value  $\rho_{\odot} = 0.43 \text{ GeV}/\text{cm}^3$  is used.

For most SM annihilation channels, we observe very good agreement between the DM interpretation of the CR antiprotons and the GCE gamma-ray flux. The preferred region in  $\langle\sigma v\rangle$  and  $m_{\text{DM}}$  is consistent when comparing the CR and GCE fits individually, and the combined CR+GCE fit. However, as can be seen in the upper left panel of figure 2, annihilation into gluons (or light quarks) is disfavored as an explanation of both the CR antiproton flux and the GCE, as both signals individually prefer different regions of DM mass. Annihilation into  $t$  quarks is also disfavored since it does not provide a good fit to either the GCE or antiprotons. Adding the constraints from dwarf galaxies disfavors large values for  $\langle\sigma v\rangle$ , but hardly affects the combined CR+GCE fit. Numerical values of the

best-fit  $\chi^2$  are reported in Table 1.

From the figure we note also that CR prefer a somewhat larger  $\langle\sigma v\rangle$  than the GCE and, hence, the joint fit pushes  $\rho_\odot$  towards slightly larger values with respect to the assumed prior from [32]. More precisely, we find, with some variation depending on the DM channel, that the global fit gives a value  $\rho_\odot = 0.55 \pm 0.15$  GeV/cm<sup>3</sup>, i.e.,  $\sim 0.1$  GeV/cm<sup>3</sup> higher than the input prior. We find that  $\rho_\odot = 0.3$  GeV/cm<sup>3</sup> is at the lower edge of  $\sim 3\sigma$  range preferred by the fit. This means that if the true  $\rho_\odot$  is significantly lower than 0.3 GeV/cm<sup>3</sup> it becomes difficult to reconcile the GCE with the CR data. Nonetheless, we also note that for  $z_h$ , the half-height of the CR propagation region in the Galaxy, we use the prior 2-7 kpc, but, since this parameter is unconstrained by the fit (see [16, 43]), values up to 10 kpc or more are allowed. Thus, since the DM signal approximately scales linearly in  $z_h$ , higher  $z_h$  values would allow, in consequence, lower  $\rho_\odot$  values, making possible a joint fit of the GCE and CRs down to a  $\rho_\odot$  value of 0.2 GeV/cm<sup>3</sup>. This issue is also further discussed in the next section within the Higgs portal fit.

channel	individual fits		joint fit	
	$\chi^2_{\text{CR}}$	$\chi^2_{\text{GCE}}$	$\chi^2_{\text{CR}}$	$\chi^2_{\text{GCE}}$
$gg$	50.3	20.8	52.0	31.6
$b\bar{b}$	45.8	21.2	47.9	23.5
$WW^{(*)}$	50.4	25.6	54.6	25.6
$ZZ^{(*)}$	45.6	25.0	45.8	25.9
$hh$	47.6	25.8	48.4	25.8
$t\bar{t}$	59.5	41.1	59.5	41.1

**Table 1.**  $\chi^2$  for the individual fits to CR and GCE as well as for the joint fit. The number of degrees of freedom for the CR and GCE fit is 163 and 22, respectively.

#### 4 Interpretation within the singlet scalar Higgs portal model

We now discuss a specific minimal model of DM, where we add a singlet scalar field  $S$  to the SM [68–70]. We will follow the analysis in [59],<sup>2</sup> with the main difference that now we include CR data.

The scalar field interacts with the SM Higgs field  $H$  through the Higgs portal operator  $S^2 H^\dagger H$ . Imposing an additional  $Z_2$  symmetry,  $S \rightarrow -S$ , the scalar particle is stable and thus a DM candidate. The Lagrangian of the scalar Higgs portal model reads

$$\mathcal{L} = \mathcal{L}_{\text{SM}} + \frac{1}{2}\partial_\mu S \partial^\mu S - \frac{1}{2}m_{S,0}^2 S^2 - \frac{1}{4}\lambda_S S^4 - \frac{1}{2}\lambda_{HS} S^2 H^\dagger H. \quad (4.1)$$

After electroweak symmetry breaking, the last three terms of the above Lagrangian become

$$\mathcal{L} \supset -\frac{1}{2}m_S^2 S^2 - \frac{1}{4}\lambda_S S^4 - \frac{1}{4}\lambda_{HS} h^2 S^2 - \frac{1}{2}\lambda_{HS} v h S^2, \quad (4.2)$$

with  $H = (h + v, 0)/\sqrt{2}$ ,  $v = 246$  GeV, and where we introduced the physical mass of the singlet field,  $m_S^2 = m_{S,0}^2 + \lambda_{HS} v^2/2$ . The phenomenology of the singlet Higgs portal model has

<sup>2</sup>An interpretation of the GCE within the singlet Higgs portal model has also been discussed in [71–73].

been extensively studied in the literature, see e.g. the recent reviews [74, 75] and references therein.

While the scalar self-coupling,  $\lambda_S$ , is of importance for the stability of the electroweak vacuum, the DM phenomenology of the scalar Higgs portal model is fully specified by the mass of the scalar DM particle,  $m_S = m_{\text{DM}}$ , and the strength of the coupling between the DM and Higgs particles,  $\lambda_{HS}$ . Even though the model is minimal, the  $S^2 H^\dagger H$  interaction term implies a rich phenomenology, including invisible Higgs decays,  $h \rightarrow SS$ , a DM-nucleon interaction through the exchange of a Higgs particle, and DM annihilation through  $s$ -channel Higgs,  $t$ -channel scalar exchange, and the  $S^2 h^2$  interactions.

The region most relevant for the DM interpretation of the CR antiproton flux and the GCE is the region  $m_S \lesssim 100 \text{ GeV}$ . As this is below the Higgs-pair threshold,  $m_S < m_h$ , annihilation proceeds through  $s$ -channel Higgs exchange only, and the relative weight of the different SM final states is determined by the SM Higgs branching ratios, independent of the Higgs-scalar coupling  $\lambda_{HS}$ . Above the Higgs-pair threshold,  $m_S \geq m_h$ , the  $hh$  final state opens up. The strength of the annihilation into Higgs pairs, as compared to  $W, Z$  or top-quark pairs, depends on the size of the Higgs-scalar coupling  $\lambda_{HS}$ . However, as shown in [59], within the scalar Higgs portal model the region above the Higgs-pair threshold that provides a good fit to the GCE (and to the CR) requires very large  $\lambda_{HS}$  which are excluded by direct detection limits. In the following, we will thus focus on DM masses  $m_{\text{DM}} < m_h$ .

We pursue two approaches. We first adopt a more model-independent point of view and consider a DM interpretation in terms of  $m_{\text{DM}}$  and  $\langle \sigma v \rangle$ . The only reference to the Higgs portal model is through the relative weight of the different SM final states, which is determined by  $m_{\text{DM}}$ . Such an analysis probes whether a certain combination of annihilation channels, considered individually in section 2 and 3, can provide a fit of the observations. Note that this kind of analysis can, in general, not be performed based on the results presented for the individual channels. Instead, we perform a dedicated fit to the CR antiproton flux, constructing the injection spectra from the spectra of the individual channels according to their relative weights. The result is shown in figure 3 (red contours), where we have marginalized over  $\rho_\odot$  and  $\log J$ . The preferred region of DM masses is around  $m_{\text{DM}} \approx 60 \text{ GeV}$ , where the Higgs portal model predicts annihilation pre-dominantly into bottom quarks,  $W$ -bosons and gluons with a weight of approximately 70, 20 and 10%, respectively. We find a  $\chi^2/(\text{number of degrees of freedom})$  of 47/163 for the Higgs portal model fit, compared to 71/165 for the fit without DM.

Performing a joint fit of the CR antiproton flux with the GCE (green contours) as well as with the GCE and dwarf galaxies (black contours) shifts the preferred region to slightly smaller masses  $m_{\text{DM}} \approx 55 \text{ GeV}$ , with a  $\chi^2/(\text{number of degrees of freedom})$  of 49/163 for the CR and 20.8/22 for the GCE. Although the best-fit point for the GCE-only fit lies at smaller masses, around  $m_{\text{DM}} \approx 45 \text{ GeV}$  (cf. [59]), the  $\chi^2/(\text{number of degrees of freedom})$  for the GCE in the joint fit is almost as good as for the GCE-only fit (which yields 19.2/22). We can draw the quite general conclusion that DM models where the annihilation is pre-dominantly into  $b\bar{b}$ ,  $WW^{(*)}$  or  $ZZ^{(*)}$  final states, or any combination thereof, provide a very good fit of the CR antiproton flux, the GCE and gamma-rays from dwarf galaxies, and point to a DM mass in the vicinity of  $m_{\text{DM}} \approx 60 \text{ GeV}$ .

We proceed with a more detailed analysis of the scalar Higgs portal model, where we take into account the various constraints on the parameter space from the Higgs invisible decay width, direct detection searches, searches for gamma-ray lines from the inner Galaxy and the DM relic density. Hence we consider the actual model parameters  $m_S = m_{\text{DM}}$  and

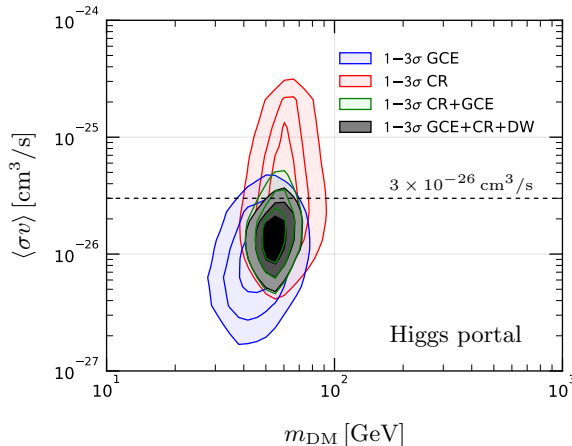


**Figure 3.** Joint fit to CR, GCE and dwarfs for the singlet scalar Higgs portal model.

$\lambda_{HS}$  defined in eq. (4.1).

We shall discuss the various constraints briefly in turn, and refer to [59] for more details.

- For light DM below the Higgs threshold,  $m_{\text{DM}} < m_h/2$ , the invisible Higgs decay  $h \rightarrow SS$  is kinematically allowed. The LHC limits on the Higgs invisible branching ratio,  $\text{BR}_{\text{inv}} \lesssim 0.23$  [76], thus imply an upper limit on the Higgs-scalar coupling  $\lambda_{HS}$  as a function of the DM mass.
- The scalar Higgs portal model predicts a spin-independent DM-nucleon scattering cross section,  $\sigma_{\text{SI}} \propto \lambda_{HS}^2/m_{\text{DM}}^2$ , through the exchange of the SM Higgs boson. The model is therefore severely constrained by direct detection experiments. We use the recent direct detection limits from LUX [77] in our numerical analysis, updating the results presented in [59]. Furthermore, we introduce the local DM density  $\rho_{\odot}$ , relevant for the DM-nucleon scattering rate and the CR flux, as an additional nuisance parameter in the fit.
- Searches for gamma-ray lines provide constraints on the cross section for the annihilation into mono-chromatic photons,  $\langle\sigma v\rangle_{\gamma\gamma}$ . We have calculated  $\langle\sigma v\rangle_{\gamma\gamma}$  using an Higgs effective Lagrangian as described in [59], and constrain the model with data from the recent Fermi-LAT search for spectral lines in the Milky Way halo [78].
- We require that the Higgs portal model provide the correct DM relic density as measured by Planck,  $\Omega h^2|_{\text{DM}} = 0.1198 \pm 0.0015$  [79]. We assume a standard cosmological history, but allow for the possibility that the dark sector is more complex than assumed within our minimal model. Hence, the DM density provided by the scalar Higgs portal model is a certain fraction,  $R \leq 1$ , of the density of all gravitationally interacting DM,  $\rho_{\text{Higgs portal}} = R \rho_{\text{DM}}$ . The total DM density predicted by our model is then  $\Omega h^2|_{\text{DM}} = \Omega h^2|_{\text{Higgs portal}}/R$ . We will consider  $R$  as a free parameter in our fit. Note that the annihilation signal today scales as  $\propto R^2$ , while the direct detection limits scale  $\propto R$ , thus implying a non-trivial interplay of the various constraints for  $R \neq 1$ .

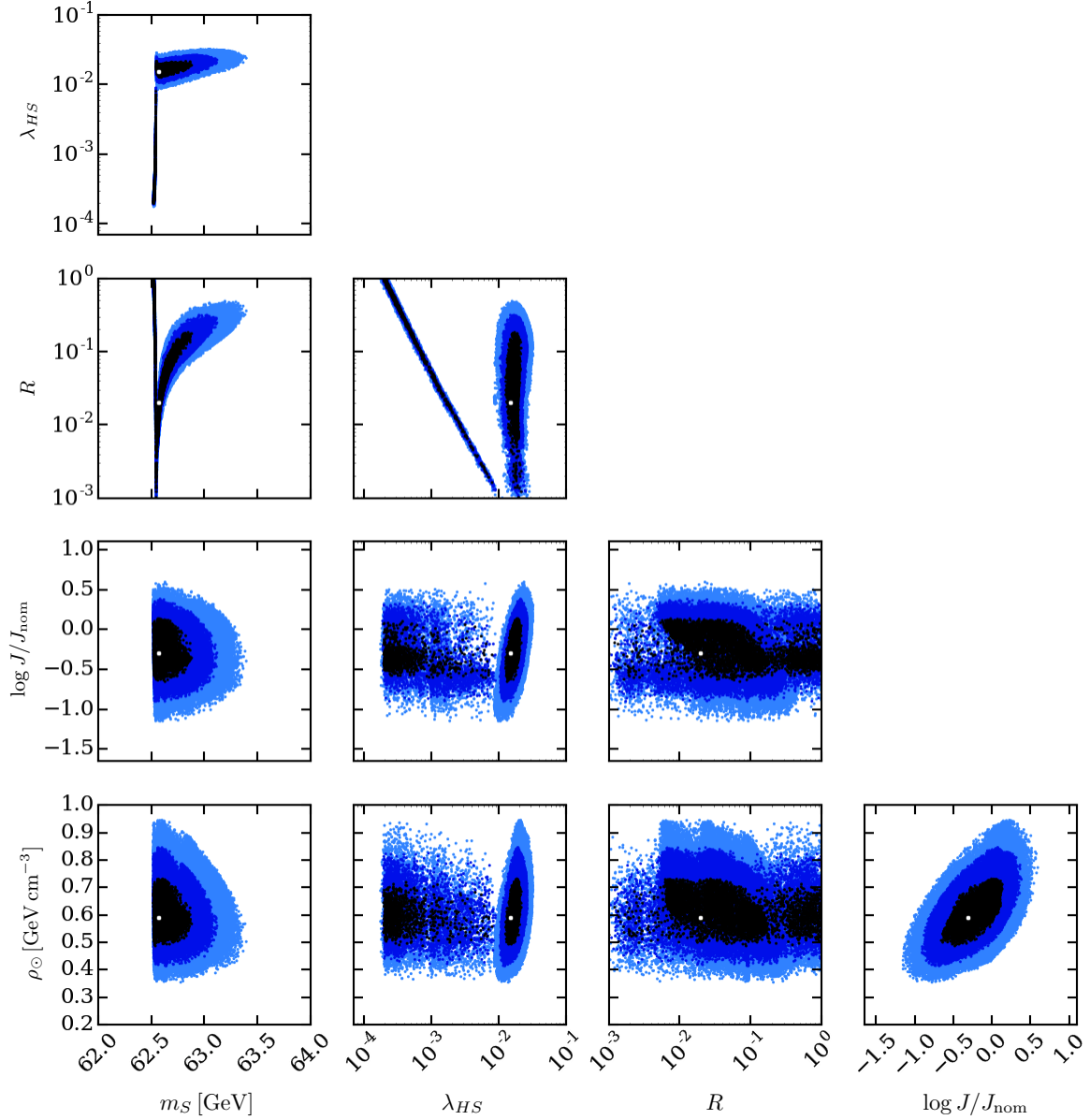


**Figure 4.** Triangle plot of the fit to the CR and GCE and all other constraints (including unconfirmed dwarfs) on the parameter space within the Higgs portal singlet scalar model. The black, blue and light blue points lie within the 1, 2, and 3 $\sigma$  region around the best-fit point (denoted by a white dot), respectively.

In figure 4 we present a fit of the Higgs portal model to the CR antiproton flux and the GCE, including the constraints from dwarf galaxies and searches for gamma-ray lines, the invisible Higgs branching ratio, direct DM detection, and the relic density.<sup>3</sup>

Let us first consider the upper left panel, which shows the allowed region in the Higgs portal coupling,  $\lambda_{HS}$ , and the DM mass. The overall flux of antiprotons and photons scales

<sup>3</sup>Compared to the analysis presented in [59] we have included the likelihood of the CR antiproton flux and updated the direct detection and dwarf galaxy limits.

with the annihilation cross section  $\langle\sigma v\rangle \propto \lambda_{HS}^2/[(m_h^2 - 4m_{\text{DM}}^2)^2 + \Gamma_h^2 m_h^2]$ , where  $\Gamma_h$  is the Higgs width. To accommodate the CR data and the GCE, either large couplings  $\lambda_{HS}$  or masses near the Higgs resonance,  $m_{\text{DM}} \approx m_h/2$ , are required. However, large couplings are excluded by the invisible Higgs branching ratio for masses  $m_{\text{DM}} \lesssim m_h/2$ , and by direct detection limits for masses  $m_{\text{DM}} \gtrsim m_h/2$ , leaving only the region near the Higgs threshold  $m_{\text{DM}} \approx m_h/2$ , where the annihilation proceeds through resonant Higgs exchange.

Upon closer inspection, we find two viable regions of parameter space, see the panel displaying the allowed region in the Higgs portal coupling and the scalar DM fraction  $R$ . In one region,  $\lambda_{HS}$  is of order  $\mathcal{O}(10^{-2})$  and  $R < 1$ , so that an additional DM component is required. In the second region, the scalar particle constitutes a significant fraction or even all of DM,  $R \lesssim 1$ , but the Higgs portal coupling must be very small, of order  $\mathcal{O}(10^{-3} - 10^{-4})$ . These two regions are a result of an interplay between the strong velocity dependence of the annihilation cross section near the resonance and the non-trivial scaling of the CR and GCE signals and the relic density with the fraction  $R$  of scalar DM.

The best-fit points as well as their  $\chi^2$  values are listed in table 2 for the two regions described above. For comparison we also show the results for the fit where we leave out the CR likelihood (GCE+constraints) or the GCE likelihood (CR+constraints). Within the Higgs portal model the observations are very well compatible with each other. However, the CR signal prefers a flux corresponding to a slightly larger annihilation cross section. In the joint fit the nuisance parameters  $\rho_\odot$  and  $\log J/J_{\text{nom}}$  leave enough freedom to accommodate both signals. In fact, for  $\rho_\odot$  and  $\log J/J_{\text{nom}}$  the fit prefers somewhat larger and smaller values, respectively, than the nominal ones (cf. lower panels in figure 4). Note that  $\rho_\odot$  also effects the direct detection rate  $\propto \rho_\odot R \lambda_{HS}^2$ . As compared to the fit of the GCE presented in [59], the improved LUX limits and, to a lesser extent, the larger DM density  $\rho_\odot$  further constrain large values of  $R$  in the first region where  $\lambda_{HS}$  is of order  $\mathcal{O}(10^{-2})$ . Another difference to the results of [59] arises from the fact that the recent results from dwarf galaxies are less constraining and, in particular, are not in tension with the GCE anymore. This allows for larger  $\langle\sigma v\rangle$  and hence for a smaller value of  $\log J/J_{\text{nom}}$  while still fitting the GCE signal. Note also that the  $\rho_\odot$  range preferred by the Higgs portal model,  $\rho_\odot = 0.6 \pm 0.1$  GeV/cm<sup>3</sup> (see figure 4), is different from the case of the single channel fits where, instead,  $\rho_\odot = 0.55 \pm 0.15$  GeV/cm<sup>3</sup>. The specific parameter region preferred by the Higgs portal fit, thus, further pushes  $\rho_\odot$  toward higher values with respect to the single channel fit case.

## 5 Conclusion

In this paper we analyze antiproton data from AMS-02 searching for a signature of DM annihilation. Using the same methodology of [16], we take into account CR propagation uncertainties by fitting at the same time DM and propagation parameters. With respect to [16] we explore a wider class of annihilation channels including  $gg$ ,  $b\bar{b}$ ,  $WW^*$ ,  $ZZ^*$ ,  $hh$  and  $t\bar{t}$ . We find that almost all the channels provide similar hints of a DM annihilation at about  $4\sigma$  level (considering statistical uncertainties only) with masses ranging from 40 and 130 GeV depending on the annihilation channel. Annihilation into  $t\bar{t}$  provides a smaller fit improvement, at the  $3\sigma$  level.

We then investigate the compatibility of the antiproton DM hint with the GCE performing a joint gamma-ray and antiproton fit where we further introduce two nuisance parameters related to the distribution of DM in the vicinity of the Galactic center and in the Solar local neighborhood. We find that the two signals are well compatible for most of the channels,

except for  $gg$ , where the two are somewhat in tension. Overall, we find that  $b\bar{b}$ ,  $ZZ^*$  and  $hh$  provides good fits to both the GCE and antiprotons, followed by  $WW^*$ , which fits only slightly worse.  $gg$  and  $t\bar{t}$  are less favored, either because they do not fit well one of the two signals or because the two signals are found to be in tension. We also include in the fit the latest results from the analysis of dwarf galaxies in gamma rays and we find that dwarf constraints are compatible with the joint GCE and antiproton fit and do not change significantly the conclusions.

Finally, as an example, we perform the above joint fit for the specific case of the Higgs portal DM model, including, in this case, also constraints from direct detection and collider searches. We find that a surviving, although fine tuned, region corresponding to DM of mass equal to about  $m_h/2$  annihilating via resonant Higgs exchange satisfies all constraints and provides a good fit to both antiprotons and gamma rays.

## Acknowledgements

We acknowledge support by the German Research Foundation DFG through the research unit “New physics at the LHC”.

## References

- [1] L. Bergstrom, J. Edsjo and P. Ullio, *Cosmic anti-protons as a probe for supersymmetric dark matter?*, *Astrophys. J.* **526** (1999) 215–235, [[astro-ph/9902012](#)].
- [2] F. Donato, N. Fornengo, D. Maurin and P. Salati, *Antiprotons in cosmic rays from neutralino annihilation*, *Phys. Rev.* **D69** (2004) 063501, [[astro-ph/0306207](#)].
- [3] T. Bringmann and P. Salati, *The galactic antiproton spectrum at high energies: Background expectation vs. exotic contributions*, *Phys. Rev.* **D75** (2007) 083006, [[astro-ph/0612514](#)].
- [4] F. Donato, D. Maurin, P. Brun, T. Delahaye and P. Salati, *Constraints on WIMP Dark Matter from the High Energy PAMELA  $\bar{p}/p$  data*, *Phys. Rev. Lett.* **102** (2009) 071301, [[0810.5292](#)].
- [5] N. Fornengo, L. Maccione and A. Vittino, *Constraints on particle dark matter from cosmic-ray antiprotons*, *JCAP* **1404** (2014) 003, [[1312.3579](#)].
- [6] D. Hooper, T. Linden and P. Mertsch, *What Does The PAMELA Antiproton Spectrum Tell Us About Dark Matter?*, *JCAP* **1503** (2015) 021, [[1410.1527](#)].
- [7] V. Pettorino, G. Busoni, A. De Simone, E. Morgante, A. Riotto and W. Xue, *Can AMS-02 discriminate the origin of an anti-proton signal?*, *JCAP* **1410** (2014) 078, [[1406.5377](#)].
- [8] M. Boudaud, M. Cirelli, G. Giesen and P. Salati, *A fussy revisitiation of antiprotons as a tool for Dark Matter searches*, *JCAP* **1505** (2015) 013, [[1412.5696](#)].
- [9] J. A. R. Cembranos, V. Gammaldi and A. L. Maroto, *Antiproton signatures from astrophysical and dark matter sources at the galactic center*, *JCAP* **1503** (2015) 041, [[1410.6689](#)].
- [10] M. Cirelli, D. Gaggero, G. Giesen, M. Taoso and A. Urbano, *Antiproton constraints on the GeV gamma-ray excess: a comprehensive analysis*, *JCAP* **1412** (2014) 045, [[1407.2173](#)].
- [11] T. Bringmann, M. Vollmann and C. Weniger, *Updated cosmic-ray and radio constraints on light dark matter: Implications for the GeV gamma-ray excess at the Galactic center*, *Phys. Rev.* **D90** (2014) 123001, [[1406.6027](#)].
- [12] G. Giesen, M. Boudaud, Y. Genolini, V. Poulin, M. Cirelli, P. Salati et al., *AMS-02 antiprotons, at last! Secondary astrophysical component and immediate implications for Dark Matter*, *JCAP* **1509** (2015) 023, [[1504.04276](#)].

- [13] H.-B. Jin, Y.-L. Wu and Y.-F. Zhou, *Upper limits on dark matter annihilation cross sections from the first AMS-02 antiproton data*, *Phys. Rev.* **D92** (2015) 055027, [[1504.04604](#)].
- [14] C. Evoli, D. Gaggero and D. Grasso, *Secondary antiprotons as a Galactic Dark Matter probe*, *JCAP* **1512** (2015) 039, [[1504.05175](#)].
- [15] AMS collaboration, M. Aguilar et al., *Antiproton Flux, Antiproton-to-Proton Flux Ratio, and Properties of Elementary Particle Fluxes in Primary Cosmic Rays Measured with the Alpha Magnetic Spectrometer on the International Space Station*, *Phys. Rev. Lett.* **117** (2016) .
- [16] A. Cuoco, M. Krämer and M. Korsmeier, *Novel Dark Matter Constraints from Antiprotons in Light of AMS-02*, *Phys. Rev. Lett.* **118** (2017) 191102, [[1610.03071](#)].
- [17] M.-Y. Cui, Q. Yuan, Y.-L. S. Tsai and Y.-Z. Fan, *Possible dark matter annihilation signal in the AMS-02 antiproton data*, *Phys. Rev. Lett.* **118** (2017) 191101, [[1610.03840](#)].
- [18] AMS collaboration, M. Aguilar et al., *Precision Measurement of the Boron to Carbon Flux Ratio in Cosmic Rays from 1.9 GV to 2.6 TV with the Alpha Magnetic Spectrometer on the International Space Station*, *Phys. Rev. Lett.* **117** (2016) 231102.
- [19] FERMI-LAT collaboration, V. Vitale and A. Morselli, *Indirect Search for Dark Matter from the center of the Milky Way with the Fermi-Large Area Telescope*, in *Fermi gamma-ray space telescope. Proceedings, 2nd Fermi Symposium, Washington, USA, November 2-5, 2009*, 2009. [0912.3828](#).
- [20] L. Goodenough and D. Hooper, *Possible Evidence For Dark Matter Annihilation In The Inner Milky Way From The Fermi Gamma Ray Space Telescope*, [0910.2998](#).
- [21] D. Hooper and L. Goodenough, *Dark Matter Annihilation in The Galactic Center As Seen by the Fermi Gamma Ray Space Telescope*, *Phys. Lett.* **B697** (2011) 412–428, [[1010.2752](#)].
- [22] D. Hooper and T. Linden, *On The Origin Of The Gamma Rays From The Galactic Center*, *Phys. Rev.* **D84** (2011) 123005, [[1110.0006](#)].
- [23] K. N. Abazajian and M. Kaplinghat, *Detection of a Gamma-Ray Source in the Galactic Center Consistent with Extended Emission from Dark Matter Annihilation and Concentrated Astrophysical Emission*, *Phys. Rev.* **D86** (2012) 083511, [[1207.6047](#)].
- [24] D. Hooper and T. R. Slatyer, *Two Emission Mechanisms in the Fermi Bubbles: A Possible Signal of Annihilating Dark Matter*, *Phys. Dark Univ.* **2** (2013) 118–138, [[1302.6589](#)].
- [25] C. Gordon and O. Macias, *Dark Matter and Pulsar Model Constraints from Galactic Center Fermi-LAT Gamma Ray Observations*, *Phys. Rev.* **D88** (2013) 083521, [[1306.5725](#)].
- [26] K. N. Abazajian, N. Canac, S. Horiuchi and M. Kaplinghat, *Astrophysical and Dark Matter Interpretations of Extended Gamma-Ray Emission from the Galactic Center*, *Phys. Rev.* **D90** (2014) 023526, [[1402.4090](#)].
- [27] T. Daylan, D. P. Finkbeiner, D. Hooper, T. Linden, S. K. N. Portillo, N. L. Rodd et al., *The characterization of the gamma-ray signal from the central Milky Way: A case for annihilating dark matter*, *Phys. Dark Univ.* **12** (2016) 1–23, [[1402.6703](#)].
- [28] F. Calore, I. Cholis and C. Weniger, *Background model systematics for the Fermi GeV excess*, *JCAP* **1503** (2015) 038, [[1409.0042](#)].
- [29] FERMI-LAT collaboration, M. Ajello et al., *Fermi-LAT Observations of High-Energy  $\gamma$ -Ray Emission Toward the Galactic Center*, *Astrophys. J.* **819** (2016) 44, [[1511.02938](#)].
- [30] C. Karwin, S. Murgia, T. M. P. Tait, T. A. Porter and P. Tanedo, *Dark Matter Interpretation of the Fermi-LAT Observation Toward the Galactic Center*, *Phys. Rev.* **D95** (2017) 103005, [[1612.05687](#)].
- [31] J. F. Navarro, C. S. Frenk and S. D. M. White, *The Structure of cold dark matter halos*, *Astrophys. J.* **462** (1996) 563–575, [[astro-ph/9508025](#)].

- [32] P. Salucci, F. Nesti, G. Gentile and C. F. Martins, *The dark matter density at the Sun's location*, *Astron. Astrophys.* **523** (2010) A83, [[1003.3101](#)].
- [33] M. Cirelli, G. Corcella, A. Hektor, G. Hutsi, M. Kadastik, P. Panci et al., *PPPC 4 DM ID: A Poor Particle Physicist Cookbook for Dark Matter Indirect Detection*, *JCAP* **1103** (2011) 051, [[1012.4515](#)].
- [34] J. Alwall, R. Frederix, S. Frixione, V. Hirschi, F. Maltoni, O. Mattelaer et al., *The automated computation of tree-level and next-to-leading order differential cross sections, and their matching to parton shower simulations*, *JHEP* **07** (2014) 079, [[1405.0301](#)].
- [35] T. Sjostrand, S. Mrenna and P. Z. Skands, *A Brief Introduction to PYTHIA 8.1*, *Comput. Phys. Commun.* **178** (2008) 852–867, [[0710.3820](#)].
- [36] A. W. Strong, I. V. Moskalenko and O. Reimer, *Diffuse continuum gamma-rays from the galaxy*, *Astrophys. J.* **537** (2000) 763–784, [[astro-ph/9811296](#)].
- [37] A. W. Strong, *Recent extensions to GALPROP*, [1507.05020](#).
- [38] AMS collaboration, M. Aguilar et al., *Precision Measurement of the Proton Flux in Primary Cosmic Rays from Rigidity 1 GV to 1.8 TV with the Alpha Magnetic Spectrometer on the International Space Station*, *Phys. Rev. Lett.* **114** (2015) 171103.
- [39] AMS collaboration, M. Aguilar et al., *Precision Measurement of the Helium Flux in Primary Cosmic Rays of Rigidities 1.9 GV to 3 TV with the Alpha Magnetic Spectrometer on the International Space Station*, *Phys. Rev. Lett.* **115** (2015) 211101.
- [40] Y. S. Yoon et al., *Cosmic-Ray Proton and Helium Spectra from the First CREAM Flight*, *Astrophys. J.* **728** (2011) 122, [[1102.2575](#)].
- [41] E. C. Stone et al., *Voyager 1 Observes Low-Energy Galactic Cosmic Rays in a Region Depleted of Heliospheric Ions*, *Science* **341** (2013) .
- [42] F. Feroz, M. P. Hobson and M. Bridges, *MultiNest: an efficient and robust Bayesian inference tool for cosmology and particle physics*, *Mon. Not. Roy. Astron. Soc.* **398** (2009) 1601–1614, [[0809.3437](#)].
- [43] M. Korsmeier and A. Cuoco, *Galactic cosmic-ray propagation in the light of AMS-02: Analysis of protons, helium, and antiprotons*, *Phys. Rev.* **D94** (2016) 123019, [[1607.06093](#)].
- [44] L. C. Tan and L. K. Ng, *Calculation of the equilibrium anti-proton spectrum*, *J. Phys.* **G9** (1983) 227–242.
- [45] M. di Mauro, F. Donato, A. Goudelis and P. D. Serpico, *New evaluation of the antiproton production cross section for cosmic ray studies*, *Phys. Rev.* **D90** (2014) 085017, [[1408.0288](#)].
- [46] M. Kachelriess, I. V. Moskalenko and S. S. Ostapchenko, *New calculation of antiproton production by cosmic ray protons and nuclei*, *Astrophys. J.* **803** (2015) 54, [[1502.04158](#)].
- [47] A. Burkert, *The Structure of dark matter halos in dwarf galaxies*, *IAU Symp.* **171** (1996) 175, [[astro-ph/9504041](#)].
- [48] FERMI-LAT collaboration, M. Ackermann et al., *The Fermi Galactic Center GeV Excess and Implications for Dark Matter*, *Astrophys. J.* **840** (2017) 43, [[1704.03910](#)].
- [49] J. Petrovic, P. D. Serpico and G. Zaharija, *Galactic Center gamma-ray "excess" from an active past of the Galactic Centre?*, *JCAP* **1410** (2014) 052, [[1405.7928](#)].
- [50] J. Petrovic, P. D. Serpico and G. Zaharijas, *Millisecond pulsars and the Galactic Center gamma-ray excess: the importance of luminosity function and secondary emission*, *JCAP* **1502** (2015) 023, [[1411.2980](#)].
- [51] I. Cholis, C. Evoli, F. Calore, T. Linden, C. Weniger and D. Hooper, *The Galactic Center GeV Excess from a Series of Leptonic Cosmic-Ray Outbursts*, *JCAP* **1512** (2015) 005, [[1506.05119](#)].

- [52] R. Bartels, S. Krishnamurthy and C. Weniger, *Strong support for the millisecond pulsar origin of the Galactic center GeV excess*, *Phys. Rev. Lett.* **116** (2016) 051102, [[1506.05104](#)].
- [53] S. K. Lee, M. Lisanti, B. R. Safdi, T. R. Slatyer and W. Xue, *Evidence for Unresolved  $\gamma$ -Ray Point Sources in the Inner Galaxy*, *Phys. Rev. Lett.* **116** (2016) 051103, [[1506.05124](#)].
- [54] FERMI-LAT collaboration, M. Ajello et al., *Characterizing the population of pulsars in the Galactic bulge with the Fermi Large Area Telescope*, *Submitted to: Astrophys. J.* (2017) , [[1705.00009](#)].
- [55] FERMI-LAT collaboration, M. Ackermann et al., *Dark matter constraints from observations of 25 Milky Way satellite galaxies with the Fermi Large Area Telescope*, *Phys. Rev.* **D89** (2014) 042001, [[1310.0828](#)].
- [56] DES, FERMI-LAT collaboration, A. Drlica-Wagner et al., *Search for Gamma-Ray Emission from DES Dwarf Spheroidal Galaxy Candidates with Fermi-LAT Data*, *Astrophys. J.* **809** (2015) L4, [[1503.02632](#)].
- [57] FERMI-LAT collaboration, M. Ackermann et al., *Searching for Dark Matter Annihilation from Milky Way Dwarf Spheroidal Galaxies with Six Years of Fermi Large Area Telescope Data*, *Phys. Rev. Lett.* **115** (2015) 231301, [[1503.02641](#)].
- [58] DES, FERMI-LAT collaboration, A. Albert et al., *Searching for Dark Matter Annihilation in Recently Discovered Milky Way Satellites with Fermi-LAT*, *Astrophys. J.* **834** (2017) 110, [[1611.03184](#)].
- [59] A. Cuoco, B. Eiteneuer, J. Heisig and M. Krämer, *A global fit of the  $\gamma$ -ray galactic center excess within the scalar singlet Higgs portal model*, *JCAP* **1606** (2016) 050, [[1603.08228](#)].
- [60] A. Geringer-Sameth, M. G. Walker, S. M. Koushiappas, S. E. Koposov, V. Belokurov, G. Torrealba et al., *Indication of Gamma-ray Emission from the Newly Discovered Dwarf Galaxy Reticulum II*, *Phys. Rev. Lett.* **115** (2015) 081101, [[1503.02320](#)].
- [61] S. Li, Y.-F. Liang, K.-K. Duan, Z.-Q. Shen, X. Huang, X. Li et al., *Search for gamma-ray emission from eight dwarf spheroidal galaxy candidates discovered in Year Two of Dark Energy Survey with Fermi-LAT data*, *Phys. Rev.* **D93** (2016) 043518, [[1511.09252](#)].
- [62] FERMI-LAT, MAGIC collaboration, M. L. Ahnen et al., *Limits to dark matter annihilation cross-section from a combined analysis of MAGIC and Fermi-LAT observations of dwarf satellite galaxies*, *JCAP* **1602** (2016) 039, [[1601.06590](#)].
- [63] A. Geringer-Sameth, S. M. Koushiappas and M. Walker, *Dwarf galaxy annihilation and decay emission profiles for dark matter experiments*, *Astrophys. J.* **801** (2015) 74, [[1408.0002](#)].
- [64] DES collaboration, J. D. Simon et al., *Stellar Kinematics and Metallicities in the Ultra-Faint Dwarf Galaxy Reticulum II*, *Astrophys. J.* **808** (2015) 95, [[1504.02889](#)].
- [65] G. D. Martinez, *A robust determination of Milky Way satellite properties using hierarchical mass modelling*, *Mon. Not. Roy. Astron. Soc.* **451** (2015) 2524–2535, [[1309.2641](#)].
- [66] V. Bonnivard et al., *Dark matter annihilation and decay in dwarf spheroidal galaxies: The classical and ultrafaint dSphs*, *Mon. Not. Roy. Astron. Soc.* **453** (2015) 849–867, [[1504.02048](#)].
- [67] J. I. Read, *The Local Dark Matter Density*, *J. Phys.* **G41** (2014) 063101, [[1404.1938](#)].
- [68] V. Silveira and A. Zee, *SCALAR PHANTOMS*, *Phys. Lett.* **B161** (1985) 136.
- [69] J. McDonald, *Gauge singlet scalars as cold dark matter*, *Phys. Rev.* **D50** (1994) 3637–3649, [[hep-ph/0702143](#)].
- [70] C. P. Burgess, M. Pospelov and T. ter Veldhuis, *The Minimal model of nonbaryonic dark matter: A Singlet scalar*, *Nucl. Phys.* **B619** (2001) 709–728, [[hep-ph/0011335](#)].
- [71] N. Okada and O. Seto, *Gamma ray emission in Fermi bubbles and Higgs portal dark matter*, *Phys. Rev.* **D89** (2014) 043525, [[1310.5991](#)].

- [72] T. Mondal and T. Basak, *Class of Higgs-portal Dark Matter models in the light of gamma-ray excess from Galactic center*, *Phys. Lett.* **B744** (2015) 208–212, [[1405.4877](#)].
- [73] M. Duerr, P. Fileviez Perez and J. Smirnov, *Gamma-Ray Excess and the Minimal Dark Matter Model*, *JHEP* **06** (2016) 008, [[1510.07562](#)].
- [74] J. M. Cline, K. Kainulainen, P. Scott and C. Weniger, *Update on scalar singlet dark matter*, *Phys. Rev.* **D88** (2013) 055025, [[1306.4710](#)].
- [75] A. Beniwal, F. Rajec, C. Savage, P. Scott, C. Weniger, M. White et al., *Combined analysis of effective Higgs portal dark matter models*, *Phys. Rev.* **D93** (2016) 115016, [[1512.06458](#)].
- [76] ATLAS collaboration, G. Aad et al., *Constraints on new phenomena via Higgs boson couplings and invisible decays with the ATLAS detector*, *JHEP* **11** (2015) 206, [[1509.00672](#)].
- [77] LUX collaboration, D. S. Akerib et al., *Results from a search for dark matter in the complete LUX exposure*, *Phys. Rev. Lett.* **118** (2017) 021303, [[1608.07648](#)].
- [78] FERMI-LAT collaboration, M. Ackermann et al., *Updated search for spectral lines from Galactic dark matter interactions with pass 8 data from the Fermi Large Area Telescope*, *Phys. Rev.* **D91** (2015) 122002, [[1506.00013](#)].
- [79] PLANCK collaboration, P. A. R. Ade et al., *Planck 2015 results. XIII. Cosmological parameters*, *Astron. Astrophys.* **594** (2016) A13, [[1502.01589](#)].

log $L$ contribution	region 1			region 2		
	GCE+constr.	CR+constr.	GCE+CR+constr.	GCE+constr.	CR+constr.	GCE+CR+constr.
$m_S$ [GeV]	$62.58^{+0.76}_{-0.04}$	$62.60^{+0.21}_{-0.06}$	$62.58^{+0.18}_{-0.03}$	$62.541^{+0.003}_{-0.016}$	$62.532^{+0.012}_{-0.009}$	$62.533^{+0.011}_{-0.011}$
$\lambda_{HS}$	$0.017^{+0.015}_{-0.003}$	$0.015^{+0.006}_{-0.002}$	$0.015^{+0.004}_{-0.001}$	$0.0016^{+0.0060}_{-0.0013}$	$0.00032^{+0.00815}_{-0.00012}$	$0.00039^{+0.00561}_{-0.00017}$
$R$	$0.019^{+0.204}_{-0.018}$	$0.041^{+0.124}_{-0.040}$	$0.020^{+0.100}_{-0.018}$	$0.021^{+0.979}_{-0.019}$	$0.39^{+0.61}_{-0.38}$	$0.29^{+0.71}_{-0.28}$
$\log J/J_{\text{nom}}$	$-0.065^{+0.341}_{-0.295}$	$-0.280^{+0.351}_{-0.793}$	$-0.303^{+0.304}_{-0.205}$	$-0.099^{+0.377}_{-0.275}$	$-0.415^{+0.468}_{-0.590}$	$-0.316^{+0.238}_{-0.201}$
$\rho_{\odot}$ [GeVcm $^{-3}$ ]	$0.43^{+0.15}_{-0.15}$	$0.56^{+0.09}_{-0.08}$	$0.59^{+0.1}_{-0.05}$	$0.43^{+0.15}_{-0.15}$	$0.56^{+0.09}_{-0.09}$	$0.59^{+0.09}_{-0.06}$
$\langle\sigma v\rangle R^2$ [ $10^{-26}$ cm $^3$ /s]	$1.36^{+0.45}_{-0.44}$	$1.89^{+0.72}_{-0.53}$	$1.73^{+0.38}_{-0.47}$	$1.36^{+0.46}_{-0.45}$	$1.87^{+0.72}_{-0.51}$	$1.70^{+0.39}_{-0.32}$
$\chi^2_{\text{GCE}}$	26.22	26.49	26.69	26.47	27.35	26.88
$\chi^2_{\text{CR}}$	52.32	48.08	48.42	57.14	48.07	48.42

**Table 2.** Fit parameters and  $\langle\sigma v\rangle R^2$  for the best fit points of region 1 and 2 taking into account the log-likelihood contributions from GCE+constraints, CR+constraints and CR+GCE+constraints. Given errors are  $1\sigma$  uncertainties. We also show the corresponding  $\chi^2_{\text{GCE}}$  and the  $\chi^2_{\text{CR}}$ .